Finite-Element Analysis of the Adhesion-Cytoskeleton-Nucleus Mechanotransduction Pathway During Endothelial Cell Rounding: Axisymmetric Model

Ronald P. Jean

Christopher S. Chen

Alexander A. Spector[1]
e-mail: aspector@bme.jhu.edu

Department of Biomedical Engineering,
The Johns Hopkins University,
Baltimore, Maryland 21205

Endothelial cells possess a mechanical network connecting adhesions on the basal surface, the cytoskeleton, and the nucleus. Transmission of force at adhesions via this pathway can deform the nucleus, ultimately resulting in an alteration of gene expression and other cellular changes (mechanotransduction). Previously, we measured cell adhesion area and apparent nuclear stretch during endothelial cell rounding. Here, we reconstruct the stress map of the nucleus from the observed strains using finite-element modeling. To simulate the disruption of adhesions, we prescribe displacement boundary conditions at the basal surface of the axisymmetric model cell. We consider different scenarios of the cytoskeletal arrangement, and represent the cytoskeleton as either discrete fibers or as an effective homogeneous layer. When the nucleus is in the initial (spread) state, cytoskeletal tension holds the nucleus in an elongated, ellipsoidal configuration. Loss of cytoskeletal tension during cell rounding is represented by reactive forces acting on the nucleus in the model. In our simulations of cell rounding, we found that, for both representations of the cytoskeleton, the loss of cytoskeletal tension contributed more to the observed nuclear deformation than passive properties. Since the simulations make no assumption about the heterogeneity of the nucleus, the stress components both within and on the surface of the nucleus were calculated. The nuclear stress map showed that the nucleus experiences stress on the order of magnitude that can be significant for the function of DNA molecules and chromatin fibers. This study of endothelial cell mechanobiology suggests the possibility that mechanotransduction could result, in part, from nuclear deformation, and may be relevant to angiogenesis, wound healing, and endothelial barrier dysfunction.
[DOI: 10.1115/1.1933997]

Introduction

Cells—whether lining the vasculature, embedded within bone, or in the inner ear—respond to perturbations in their local mechanical environment [1–3]. These cellular changes that are brought about by mechanical cues (mechanotransduction) are critical to the physiology and pathology of many tissues. Endothelial cells lining blood vessels are an interesting system for the study of mechanotransduction. *In vivo*, they are continuously exposed to mechanical stimuli, including pulsatile flow of blood across their apical surface, and tensile stresses due to vessel expansion on their basal surface. These stresses can activate the G-protein signaling cascade [4], as well as cause changes to adhesions on the basal surface [5,6], and play an important role in vascular biology.

In the endothelial cell, as well as in many other cell types, many subcellular structures between the outer cellular surface and innermost regions of the cell are mechanically connected. Directly relevant to mechanotransduction, integrins at the surface of endothelial cells are mechanically coupled to the nucleus by way of the cytoskeletal network [7]. This adhesion-cytoskeleton-nucleus pathway provides a direct line of force transfer for mechanical perturbations on the surface of the cell to propagate to the nucleus, raising the possibility that mechanotransduction might occur within or near the nucleus. Changes in nuclear shape as a result of changes in cell shape appear to alter gene expression and protein synthesis [8]. Thus, a quantitative characterization of the forces acting within and/or on the nucleus may provide insight to endothelial cell mechanotransduction.

The forces deforming the nucleus could have several effects of biochemical nature: First, they can change the binding rates of the molecules involved in DNA synthesis and gene transcription; second, these forces can cause changes in DNA molecules and chromatin fibers, and third, they could affect transport on mRNA molecules through the nuclear pores. It has been shown that if a force applied to a DNA molecule becomes greater than 10 pN, the molecule behaves as if it changes its chemical structure, and if the force reaches 65 pN, the molecule yields and overstretches [9]. If torsional stresses are applied to a molecule of DNA, and the torque reaches 9 pN $\times$ nm, the molecule locally denatures releasing torsional stress [10]. When the torque increases up to 20 pN nm, the DNA molecule adopts a new overtwisted structure [11]. Cui and Bustamante (2000) extended a single chromatin fiber, and found that if the applied force reached 5–6 pN, the fiber undergoes a structural transition [12]. If the chromatin fiber is extended by a force greater than 20 pN, nucleosomes become unraveled [13]. *In vitro* studies of RNA and DNA polymerases show that these motors can develop forces up to 30–40 pN [14]. Thus, mechanical stresses experienced at the nucleus in living cells may affect nuclear processes.

Previously, we performed experiments to investigate the deformations of the nucleus resulting from endothelial cell rounding

[1]Corresponding author.
Contributed by the Bioengineering Division for publication in the JOURNAL OF BIOMECHANICAL ENGINEERING. Manuscript received: July 26, 2004; revision received: January 20, 2005. Associate Editor: Jay D. Humphrey.

[15]. Adhesion area was altered by disruption of integrin binding. We calculated nuclear stretch in response to changes in projected cell area (apparent adhesion area). We found that stretches of the major and minor axes of the projected nuclear area had the same mean value (0.69). Moreover, the rate of nuclear and projected area change was similar, suggesting a direct and immediate response of the nucleus to changes in adhesion area. We used an analytical approach and estimated the stress field, and then estimated the magnitude of force for a hypothetical arrangement of the deformation forces, and found them to be on the same order of magnitude as adhesion forces.

Here, we extend our study of the adhesion-cytoskeleton-nucleus mechanical pathway by considering a computational, finite-element model of cell rounding. This version of the model is axisymmetric. We use the major elements of the cell (nucleus, cytoskeleton, cytoplasm, cortical layer), and incorporate the latest mechanical properties of each structure. We found that passive properties did not contribute much to the nuclear deformation. Rather, most of the deformation of the nucleus during cell rounding was due to a loss of cytoskeletal pretension (treated as reactive forces in our model). The model was robust, being insensitive to changes in geometry, cytoskeletal material properties, and cytoskeletal arrangement. We applied our model to compute the stresses inside and along the nucleus that are generated during endothelial cell rounding, which might be important for mechanotransduction in the nucleus. These results may lead to a better understanding of wound healing, angiogenesis, and endothelial barrier dysfunction.

Model

Constitutive Relations. Our model includes the major subcellular structures (nucleus, cytoskeleton, cytosol, cortical layer) that are treated as incompressible neo-Hookean materials, whose strain energy function U is given by the equation

$$U = C_{10}(\lambda_1^2 + \lambda_2^2 + \lambda_3^2 - 3) \tag{1}$$

Here C_{10} is a constant and λ_1, λ_2, and λ_3 are the principal stretches. The constant C_{10} is related to Young's E modulus by the equations

$$C_{10} = E/6 \tag{2}$$

In terms of the cytoskeleton, the above constitutive relation describes its passive properties, and the active properties of the cytoskeleton will be considered below.

Model Parameters. Our model axisymmetric cell possessed a maximum diameter of 20 microns, and a maximum height of 8 microns. The model nucleus had a maximum radius of 8 microns, and a height of 4 microns. The cortical layer of the cell had a thickness between 0.2–0.4 microns. These dimensions were representative of our experimental data in [15], and are consistent with other studies on endothelial cells [16]. The Young's moduli used for the nucleus, cytoskeleton, cytosol, and cortical layer were 5000 Pa, 500–1500 Pa (see Discussion), 500 Pa, and 1000 Pa, respectively.

The magnitude of the computational reactive forces used in each case was chosen as follows. In the case of the discrete cytoskeletal fiber simulations, 17 point forces were prescribed along the arc of the nucleus between ±45 deg for an adhesion area fraction=0.4. Forces were chosen to produce a stress field of roughly 2000 Pa on the surface of the nucleus, consistent with previous estimates [15]. We apply roughly one force per each node of the fiber cross section (3 elementary computational forces per fiber). The nodewise (instead of fiberwise) application of the forces was used to help avoid local inhomogeneity in the deformation of the nucleus that caused difficulties in the comparison with the data of our experiment [15] (see also the Computational Method). For simulations with higher values for the adhesion area fraction, fewer forces were used, proportional to the number of released fibers (as described above). In the case of the effective

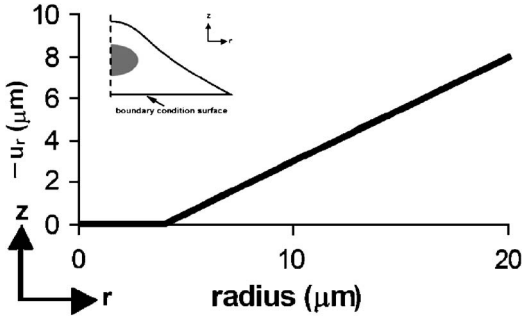

Fig. 1 The boundary condition to simulate detachment of the cell surface from the substrate during cell rounding. The case of an adhesion area fraction=0.4 is considered, and the jump in the radial component of the cell displacement as a function of the cell radius is prescribed.

layer representation of the cytoskeleton, 17 point forces were also prescribed along the arc of the nucleus between ±45 deg for an adhesion area fraction=0.4. For simulations with higher values for the adhesion area fraction, all 17 point forces were kept. However, the magnitudes of the forces were chosen to be consistent with stress fields estimated previously for these different states [15]. Forces were inclined between 17 and 19 deg from the horizontal in order to correspond with cytoskeletal fiber orientation.

Boundary Conditions: Model of Cell Detachment. To simulate endothelial cell rounding, we imposed the boundary condition that describes the detachment of a portion of the cell surface. The cell surface detachment was modeled as a jump in the radial (in-plane) component of the cell boundary elastic displacement (we did not assume any jump in the normal component of the cell displacement). The length of the detached portion of the cell surface at the current moment of time is assumed to be proportional to the time of cell rounding until that moment. As an example, Fig. 1 shows the jump in the radial displacement as a function of the radial coordinate at the moment of time when 40% of the initial adhesion area remains. The adhesion area fraction refers to the current area at the base of the cell divided by the reference spread area (e.g., adhesion area fraction=1.0 is the spread state). In the case of higher adhesion area ratios (corresponding to a cell that is more spread), the maximum displacement is lower in magnitude, but the linear decrease in displacement towards the center of the cell is maintained. In our simulations, the maximum diameter of the cell was 20 microns, and the cortical layer of the cell had a thickness between 0.2–0.4 microns.

Model of Cytoskeletal Fibers. Our concept of the forces deforming the nucleus in the process of cell rounding is based on observation of the "preprocess" of cell spreading. There is common understanding that the cell spreading is accompanied by stressing of cytoskeletal fibers, probably, via signaling from the adhesion sites that triggers the actin/myosin machinery. The actin cytoskeleton surrounds the nucleus, and may be tethered to it. Thus, we assume that in the preprocess of cell spreading the nucleus is deformed as a result of the generated cytoskeletal tension. If now we consider the process of cell rounding, we assume that the part of the cytoskeletal fibers associated with the detached part of the cell surface lose their tension. In our model of the deformation of the nucleus caused by cell rounding, the reference state is the spread state, and the current state is the partially or fully round state. Thus, the loss of the fiber pretension is equivalent to application of reactive forces to the nucleus. Our hypothetical model for the adhesion-cytoskeleton-nucleus mechanical pathway in the context of cell rounding is shown in Fig. 2. Figure 2(*a*) shows the initial (spread) state of the cell where the cytoskeletal fibers (solid lines) generate tension on the nucleus, and ultimately, form connections with the adhesion site. Figure 2(*b*) represents an

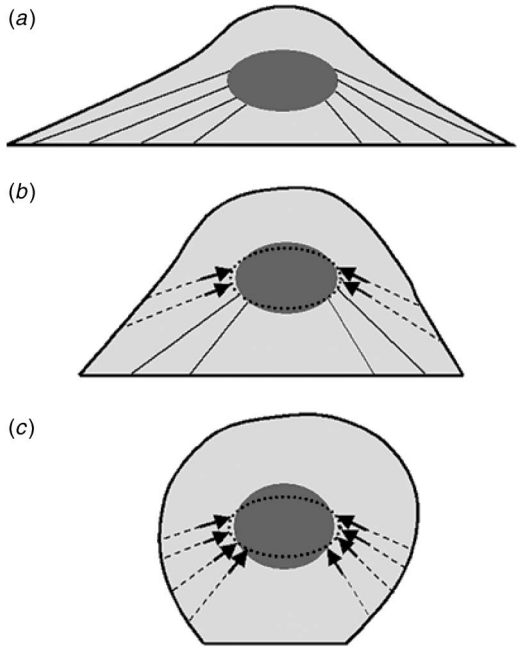

Fig. 2 Concept of the active forces associated with a loss of cytoskeletal tension in the cytoskeletal fibers due to loss of adhesion area: (*a*) reference spread state where the solid lines represent the originally stressed fibers connecting the nucleus to the adhesion sites, (*b*) intermediate state where a portion of the fibers is detached and associated with the reactive stresses (dashed lines); and, the rest of the fibers (solid lines) is still attached to the adhesion sites, and (*c*) preround state where all the fibers are associated with the reactive stresses.

intermediate (partially detached) state of the cell. When adhesions are disrupted, there is a loss of cytoskeletal tension that is represented by reactive stresses. In the considered state of the cell, such loss of the original tension occurs along a portion of the fibers that become detached from the substrate. These fibers are represented by the dashed lines in Fig. 2(*b*). Figure 2(*c*) shows a preround state of the cell where all the fibers (given in dashed lines) are detached from the substrate and associated with the reactive stresses.

The stress–strain state that we compute is determined by the deformation accompanying the transition of the cell from the spread to the round state. In our simulation of the cell and nucleus rounding, we assume that the active forces acting on the nucleus are equal in magnitude and opposite in the direction to those that were generated in the cytoskeletal fibers in the preprocess of cell spreading [Fig. 2(*c*)]. A similar concept is used in the treatment of intermediate states where the active force is associated with a portion of the fibers that become detached by the moment of time under consideration [Fig. 2(*b*)]. Thus, the mechanics of the actin cytoskeleton is determined by superposition of the active and passive properties.

To introduce the cytoskeletal fiber arrangement, we considered two cases: (1) the presence of direct cytoskeletal fiber connections from the adhesion site to the nucleus [Fig. 3(*a*)]; and, (2) a layer representing the effective material properties of a random arrangement of cytoskeletal fibers [Fig. 3(*b*)]. In the former case, the cytoskeleton is composed of almost parallel fibers with one-to-one connection between the points along the surface of the nucleus and those at the adhesion area. In the latter case, the cytoskeleton is organized in a chaotic fashion where a point at the adhesion surface can be connected to multiple points located at the surface of the nucleus. In the case of discrete fibers [Fig. 3(*a*)], reactive forces were only present on the nuclear surface if opposite fiber ends were in the displacement region. For example, if we were

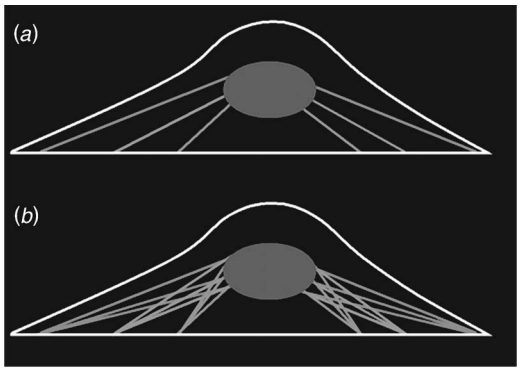

Fig. 3 Arrangement of cytoskeletal fibers in the computational cell model using (*a*) discrete fiber, and (*b*) effective layer representations

looking at a state where the maximal cell displacement was 2 microns, only the rightmost fiber in Fig. 3(*a*) would be affected, so reactive forces would only occur at the nuclear surface near the rightmost fiber. Thus, the number of forces—not force magnitude—was different between states using discrete fibers. In the case of an effective random fiber layer, we applied the same number of forces along the surface of the nucleus for any deformation state, but varied the magnitude of those forces. This scenario was meant to represent a recruitment of reactive forces as the cell became more rounded.

Computational Method

Computational simulations were performed on a personal computer running the Windows XP operating system. Two commercial software packages were used for creating the geometries of the different subcellular components and for running the finite-element analysis.

Creation of orphan mesh geometries was done using the software package, SolidWorks Student Edition 2004 (SolidWorks Co.). Individual model parts for the nucleus, cytoskeletal fibers, cytosol, and cortical layer were generated at a $1000\times$ scale, and were saved as ACIS.sat files for importation into the finite-element software package.

Finite-element analysis is a computational method whereby continuous, deformable objects are broken down into representations with a discrete number of interconnected nodes. The Complete ABAQUS Environment (CAE) version 6.3 (ABAQUS, Inc.) was used to perform the axisymmetric finite-element analysis of cell rounding. Model geometries were imported into the CAE, where they were given spatial coordinates and assigned material properties. The different parts were assigned axisymmetric, quadrilateral element types, meshed, and boundary conditions were specified. After performing the finite-element analysis, simulation outputs were viewed using the Visualization tools.

In the performed simulations, the nucleus was very constrained, due to the multiple contact-type boundary conditions that ensured mechanical continuity between the nucleus and the subcellular structures (cytosol, cytoplasm, fibers or effective layer). This resulted in the convergence of the simulations only with a mesh density for the nucleus that was lower than that for the rest of the cellular model. In order to resolve the nodal mismatch at the interface between the nuclear surface and the surrounding structures, it was necessary to perform node wise application of the active force determined by the mesh of the nucleus (see the Model Parameters).

Results and Discussion

Description of the Results. The results of our finite-element analysis are given in Figs. 4–8 and Tables 1 and 2. Figures

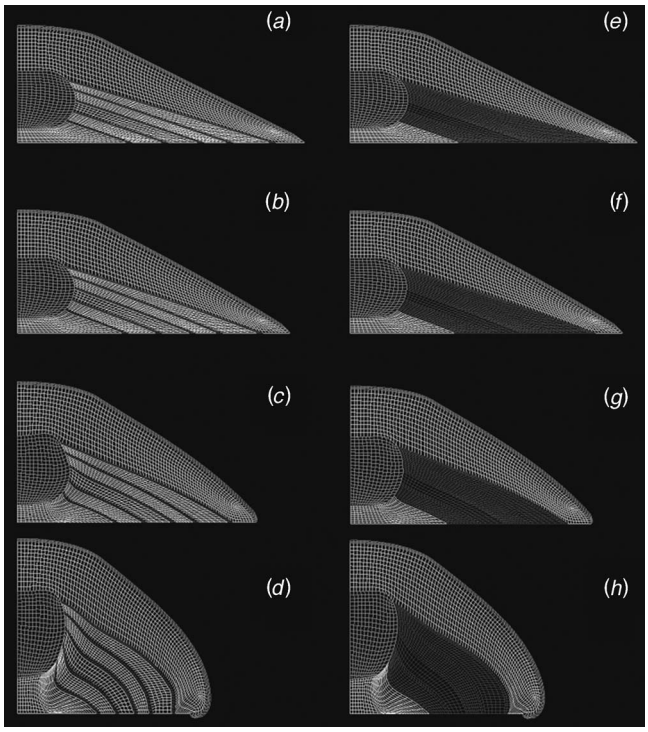

Fig. 4 Computational simulation of cell rounding for different states and different cytoskeletal configurations. Adhesion area fractions of (*a*) 1.0, (*b*) 0.9, (*c*) 0.7, and (*d*) 0.4 correspond to simulations with discrete cytoskeletal fibers. Simulations incorporating an effective layer representation of the cytoskeleton are shown for adhesion area fractions of (*e*) 1.0, (*f*) 0.9, (*g*) 0.7, and (*h*) 0.4.

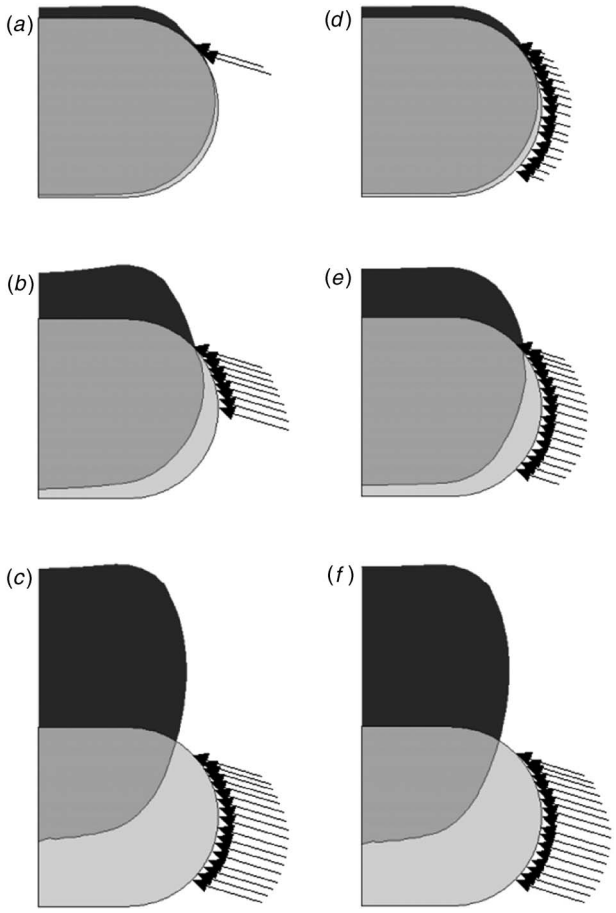

Fig. 5 Undeformed (dark) and deformed (light) states of the nucleus with prescribed reactive forces for different states and different cytoskeletal configurations. Adhesion area fractions of (*a*) 0.9, (*b*) 0.7, and (*c*) 0.4 correspond to simulations with discrete cytoskeletal fibers. Simulations incorporating an effective layer representation of the cytoskeleton are shown for adhesion area fractions of (*d*) 0.9, (*e*) 0.7, and (*f*) 0.4.

4(*a*)–4(*d*) shows the simulation results as the cell rounds for the discrete cytoskeletal fiber arrangement, and Figs. 4(*e*)–4(*h*) show different states during the rounding event for the effective layer representing a random arrangement of cytoskeletal fibers. In both scenarios for the cytoskeleton, the adhesion area fraction=0.4 corresponds to the closest state to a fully round cell in the simulations. While Fig. 4 shows the deformation of the nucleus, cytoskeletal, and whole cell during cell rounding, Figs. 5(*a*)–5(*f*) present the corresponding time evolution of the active forces deforming the nucleus. Table 1 compares the radial nuclear stretch calculated from experiments on cell rounding in [15] with the nuclear stretch from the simulations.

To investigate the contribution of purely passive properties to nuclear deformations during cell rounding, we ran the finite-element analysis as above, but removed all active forces. Thus, the nuclear deformation observed during the passive analysis would be due to bulk motion of the different materials and their properties. In Table 2, the radial nuclear stretch from the passive simulations is compared to the predicted value based on experimental data in [15].

One of the major goals of our simulations was to obtain stress maps for the nucleus. Figure 6 shows the Cauchy stress component of the nucleus, S_{11}, for an adhesion area fraction=0.4 during the cell rounding. Figure 6(*a*) shows the discrete cytoskeletal fiber simulation, while Fig. 6(*b*) relates to the simulation using the effective layer representation of the cytoskeleton. Likewise, Fig. 7 shows the nuclear stress component, S_{22}, for different cytoskeletal configurations, while Fig. 8 represents the results for the nuclear shear stress component, S_{12}.

Model Discussion. In this study, we concentrated on the force (stress) transmission along the adhesion-cytoskeleton-nucleus mechanotransduction pathway with the ultimate goal to estimate the stress field inside the nucleus and along its surface. To accomplish this, we created a finite-element model of the cell. This model cell possessed all major features of the cell, such as the nucleus, cytoskeleton, cytosol, and cortical layer. Additionally, we varied both active (reactive forces) and passive (arrangement and magnitude of the actin cytoskeleton) properties to verify if our model was robust.

The material properties used in our simulations for each sub-

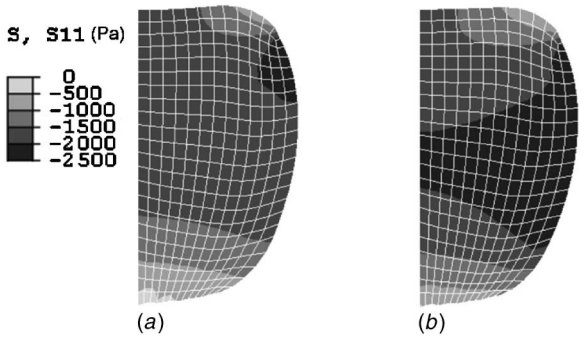

Fig. 6 Nuclear stress field of Cauchy stress component, S_{11}, corresponding to an adhesion area fraction=0.4 for (*a*) discrete fiber and (*b*) effective layer representations of the cytoskeleton

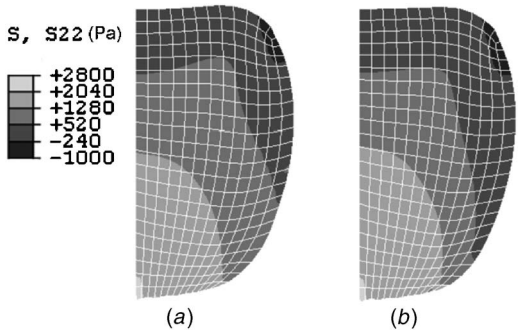

Fig. 7 Nuclear stress field of Cauchy stress component, S_{22}, corresponding to an adhesion area fraction=0.4 for (*a*) discrete fiber and (*b*) effective layer representations of the cytoskeleton

cellular structure were based upon the experimental latest measurements for endothelial cells. The Young's modulus of the nucleus was approximated to be 5000 Pa, and the Young's modulus of the cytosol used was 500 Pa, consistent with the measurements by [16,17]. For the cortical layer and cytoskeleton, we used a range of stiffness between 500–1500 Pa to determine the extent of the effect on the nuclear deformation. In our simulations, changing these properties did not cause more than a 0.01 change in nuclear stretch across the range, i.e., the effect was minimal.

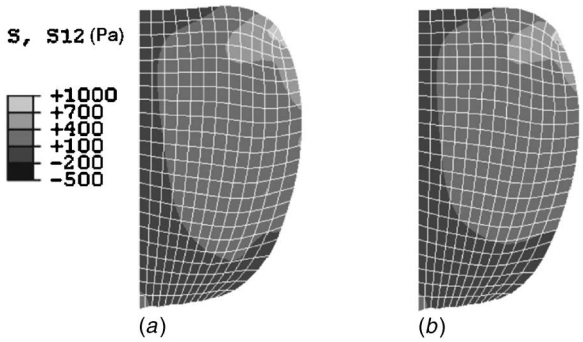

Fig. 8 Nuclear stress field of Cauchy shear stress component, S_{12}, corresponding to an adhesion area fraction=0.4 for (*a*) discrete fiber and (*b*) effect layer representations of the cytoskeleton

Table 1 Experimental and computational nuclear stretches for different times during the cell rounding event

	Nuclear stretch		
Adhesion area ratio	Predicted (experimental data)	Simulation (discrete fibers)	Simulation (effective layer)
0.9	0.96	0.97	0.97
0.7	0.88	0.91	0.91
0.4	0.80	0.82	0.82

Table 2 Experimental and computational nuclear stretches for different times during the cell rounding event in the case of no reactive force (passive properties only)

	Nuclear stretch		
Adhesion area ratio	Predicted (experimental data)	Simulation[a] (discrete fibers)	Simulation[a] (effective layer)
0.9	0.96	0.99	0.99
0.7	0.88	0.97	0.96
0.4	0.80	0.93	0.91

[a]Simulations use passive properties only

In our model, we chose the parameters on the bases of several lines of experimental data [7,15,16]. In addition to that, the results of our modeling are consistent with independent experiments. The forces acting on the nucleus are on the same order of magnitude (tens of nanonewtons) as traction forces measured by several independent groups [18–20]. Also, it can be shown, that the proposed model can reproduce the data on cell (nucleus) rounding present in [21].

Figure 3 shows two scenarios of actin cytoskeleton arrangement in our simulations. The discrete fiber representation consisted of 5 "effective" cytoskeletal fibers that, although much larger in diameter than an actual cytoskeletal filament, suffice to reflect the passive properties in this instance. The effective layer treatment of the cytoskeleton was meant to reflect a very dense, random arrangement of actin filaments, thereby allowing representation of this subcellular region with a homogenous layer.

In our model, the mesh density was such that the internodal spacing represented no greater than 0.30 microns (in most regions, the spacing was less). The simulations were also run using a lower mesh density (0.5 micron internodal spacing) to determine if this had any effect. In both cases, the results were similar, except for a larger edge effect at the leading edge of the cell in the lower density case.

To determine the dependence on geometry—and whether or not the edge effect produced any impact on the nuclear deformation—we also tried running our scenarios with a cell that had a half-trapezoidal shape (as opposed to the smooth contour of the model cell shown in the figures). This half-trapezoidal cell had more cytoplasm closer to the nucleus. However, the simulations with this other model cell produced identical nuclear deformations, indicating that the cell geometry had a minimal effect. Moreover, since there was no effect by this region near the nucleus, this suggested that the edge effect in the simulations—the leading edge of the cell being farther away than this tested region—probably had no effect on the nuclear deformation as well.

The finite-element model in this paper was axisymmetric. The assumption of axisymmetry is consistent with our earlier experimental finding [15] that the nuclear stretch along the major and minor axes of the elliptical nuclear projected area had the same mean value. Some of the effects, such as shape of the adhesion and that of the cell in the spread state could be of a 3D nature, and it will require a next-level computational model in the future. Also, the boundary conditions that simulate the detachment of the cell surface of the substrate (Fig. 1) are in terms of the vertical component of the displacement only, which causes the cell in the model to "round up." This seems a good approximation at the cellular level, but depicting the events at a molecular level might require more sophisticated boundary conditions.

Simulation of Cell Rounding. The results of our simulations for different states during cell rounding and different cytoskeletal arrangements are shown in Fig. 4. The left column of simulations, (*a*)–(*d*), represents the discrete cytoskeletal fiber simulations for adhesion area fractions of 1.0, 0.9, 0.7, and 0.4, respectively. Similarly, (*e*)–(*h*) shows the results of the simulations using the effective layer representation of the cytoskeleton for adhesion area fractions of 1.0, 0.9, 0.7, and 0.4, respectively. As one can see, the nucleus gets more and more deformed as the cell rounds: it is compressed in the directions parallel to the substrate and elongates in the perpendicular direction, which is consistent with incompressibility of the nuclear material. As a result, the nuclear shape changes from elliptical to spherical. In the case of the effective layer simulations, the deformation of the nucleus is more uniform. In addition to the deformation, the nucleus moves as a whole away from the substrate in response to cell rounding. While the stretches of the relatively stiff nucleus do not exceed 20%, the

distortion of the softer cytoskeleton is quite large [Figs. 4(*d*) and 4(*h*)]. In this modeling, the materials of the cellular components were considered elastic and incompressible. In our previous analytical treatment [15], we analyzed the effect of slight compressibility of the nuclear material and found it not very significant in terms of the forces acting on and stress inside the nucleus. Also, the relaxation time of the endothelial cell nuclei is not available at this time, but it has been found in some other cells. For example, that of the nuclei in chondrocytes was found close to 25 s [22]. Such times are much shorter than the duration of the experiment that we modeled here (about 180 s). Thus, in our case, we can treat the material of the nucleus as elastic with the short-term moduli. More general models of the nucleus used on different time scales will probably require a consideration of dissipative processes as well as two-phase (chromatin and intranuclear liquid) nature of the nuclear content.

The active forces corresponding to different moments of time during cell rounding are given in Fig. 5. Table 1 summarizes the maximal radial stretch of the nucleus in the simulations of Fig. 4 with the expected stretch value based on the experiments in [15]. As one can see, the stretch values from the simulations are very close to the predicted values from experiments. Moreover, the stretch values from both cytoskeleton scenarios are similar, with a difference between the two of less than 1%. The fact that two different representations of the cytoskeleton result in a similar nuclear deformation (nuclear stretch) suggests that our model is robust.

In order to analyze the significance of the active forces to the deformation of the nucleus, we developed a computational test when these forces are excluded, and the cell is deformed due to the passive stresses resulting from the detachment of the cellular surface from the substrate. While full-scale finite element computations of this hypothetical case are not presented, Table 2 summarizes the maximal radial stretch of the nucleus for the passive-case simulations corresponding to different stages of cell rounding. Comparing the passive results to the predicted values of stretch, one can see that passive properties alone cannot account for the nuclear deformation. Moreover, if one compares the data in Table 2 to that in Table 1, it is clear that most of the stretch (50%–70%) of the nucleus during cell rounding is a product of the loss of cytoskeletal tension (active force production in the spread state). This is consistent with earlier studies on the contractile machinery of cells (e.g., [23,24]).

Nuclear Stresses and Their Significance. In Figs. 6–8, we present the components of the nuclear stress that corresponds to an adhesion area fraction=0.4, a moment of time close to full cell rounding, where cases (*a*) and (*b*) correspond, respectively, to the "discrete-fiber" and "chaotic-fiber" model of the cytoskeleton. In Fig. 6, the radial, S_{11}, component is shown. The stress field of the nucleus for S_{11} is more uniform in the second (chaotic-fiber composition) scenario, though the magnitude of stress in each is within the same range. Figures 7 and 8 show the vertical, S_{22}, and shear, S_{12}, nuclear stress components, respectively. In each case, the discrete fiber scenario (*a*) and effective layer representation (*b*) of the cytoskeleton are very close in stress distribution. In the case of S_{22}, the magnitude of stress appears greater towards the bottom center region of the nucleus, while in the case of shear stress, S_{12}, the greater magnitude of stress is concentrated near the outer top region of the nucleus. In the case of the radial component, an average value of that throughout the nucleus is 2000 Pa. For the vertical and shear component, average values are about 2000 and 500 Pa, respectively.

From a biological point of view, the major goal of studying mechanotransduction is to understand how the mechanical forces result in biochemical signals, particularly ones associated with alterations of gene expression and protein synthesis [8,25]. The molecules of DNA are stored in the chromatin in an extremely twisted and bent form associated with intrinsic stresses, to which DNA molecules are very sensitive. DNA replication and gene transcription is associated with the binding of enzymes (polymerizes) that induce changes in the molecular stress. Protein synthesis occurs as a result of transport of mRNA molecules through nuclear pores. In order to understand the potential significance of the computed nuclear stresses for gene alteration and protein synthesis, we estimated the corresponding forces and moment (torque) that would act on a single chromatin fiber and molecule of DNA if they were in the stress field presented in Figs. 6–8. While this analysis will be published elsewhere, we found that the level of the total force acting on a representative (30-nm-diam) chromatin fiber is about 20 pN. This is above thresholds observed in experiments with isolated fibers, at which structural changes occur [12,13]. Such forces can also significantly change the rate of binding of regulatory proteins to DNA molecules [26]. In addition to the total force or torque, the perturbation of a molecule inside nucleus can be characterized in terms of changes in the molecular free energy. Thus, the computed mechanical characteristics (stresses and strains) can be converted into the corresponding free energy changes per molecule that is associated with the cell evolution during its rounding. Notice that these conclusions correspond to the adhesion area fraction=0.4, which means that even a partial detachment (rounding) of the cell can cause significant changes in the genetic material inside the nucleus. It is also important to obtain all components of the stress field because all of them contribute to the force, torque, and free energy per molecule, and each of them can be critical to the state of the molecule.

We developed a robust finite-element model to analyze the adhesion-cytoskeleton-nucleus mechanotransduction pathway during endothelial cell rounding. By using the known properties of cellular components, we reproduced the same level of nuclear deformation in our simulations as that observed in previously published experimental data. The active forces associated with the loss of cytoskeletal tension was the major cause of the nuclear deformation. Thus, passive mechanics alone did not account for the observed nuclear deformation during cell rounding. Finally, we computed the stress components inside and along the nucleus, and found that they can be significant to genetic processes in the nucleus.

Acknowledgments

The authors would like to thank the Whitaker Foundation, NIBIB (EB00262), and NHLBI (HL73305) for partial support of this investigation.

References

[1] Davies, P. F., Barbee, K. A., Volin, M. V., Robotewskyj, A., Chen, J., Joseph, L., Griem, M. L., Wernick, M. N., Jacobs, E., Polacek, D. C., dePaola, N., and Barakat, A. I., 1997, "Spatial Relationships in Early Signaling Events of Flow-Mediated Endothelial Mechanotransduction," Annu. Rev. Physiol., **59**, pp. 527–549.

[2] Brighton, C. T., Fisher, J. R., Levine, S. E., Corsetti, J. R., Reilly, T., Landsman, A. S., Williams, J. L., and Thibault, L. E., 1996, "The Biochemical Pathway Mediating the Proliferative Response of Bone Cells to a Mechanical Stimulus," J. Bone Jt. Surg., Am. Vol., **78A**, pp. 1337–1347.

[3] Brownell, W. E., Spector, A. A., Raphael, R. M., and Popel, A. S., 2001, "Micro- and Nanomechanics of the Cochlear Outer Hair Cell," Annu. Rev. Biomed. Eng., **3**, pp. 169–194.

[4] Gudi, S., Nolan, J. P., and Frangos, J. A., 1998, "Modulation of GTPase Activity of G Proteins by Fluid Stress and Phospholipid Composition," Proc. Natl. Acad. Sci. U.S.A., **95**, pp. 2616–2619.

[5] Mathur, A. B., Truskey, G. A., and Reichert, W. M., 2000, "Atomic Force and Total Internal Reflection Fluorescence Microscopy for the Study of Force Transmission in Endothelial Cells," Biophys. J., **78**, pp. 1725–1735.

[6] Mathur, A. B., Truskey, G. A., and Reichert, W. M., 2000, "Total Internal Reflection Microscopy and Atomic Force Microscopy (TIRFM-AFM) to Study Stress Transduction Mchanisms in Endothelial Cells," Crit. Rev. Biomed. Eng., **28**, pp. 197–202.

[7] Maniotis, A. J., Chen, C. S., and Ingber, D. E., 1997, "Demonstration of Mechanical Connections Between Integrins, Cytoskeletal Filaments, and Nucleoplasm that Stabilize Nuclear Structure," Proc. Natl. Acad. Sci. U.S.A., **94**, pp. 849–854.

[8] Thomas, C. H., Collier, J. H., Sfeir, C. S., and Healy, K. E., 2002, "Engineering Gene Expression and Protein Synthesis by Modulation of Nuclear Shape,"

Proc. Natl. Acad. Sci. U.S.A., **99**, pp. 1972–1977.
[9] Zlatanova, J., and Leuba, S. H., 2002, "Stretching and Imaging Single DNA Molecules and Chromatin," J. Muscle Res. Cell Motil., **23**, pp. 377–395.
[10] Strick, T. R., Allemand, J. F., Bensimon, D., and Croquette, V., 1998, "Behavior of Supercoiled DNA," Biophys. J., **74**, pp. 2016–2028.
[11] Allemand, J. F., Bensimon, D., Laverly, R., and Croquette, V., 1998, "Stretched and Overwound DNA form a Pauling-Like Structure with Exposed Bases," Proc. Natl. Acad. Sci. U.S.A., **95**, pp. 14152–14157.
[12] Cui, Y., and Bustamante, C., 2000, "Pulling a Single Chromatin Fiber Reveals the Forces that Maintain its Higher-Order Structure," Proc. Natl. Acad. Sci. U.S.A., **97**, pp. 127–132.
[13] Brower-Toland, B. D., Smith, C. L., Yeh, R. C., Lis, J. T., Peterson, C. L., and Wang, M. D., 2002, "Mechanical Disruption of Individual Nucleosomes Reveals a Reversible Multistage Release of DNA," Proc. Natl. Acad. Sci. U.S.A., **99**, pp. 1960–1965.
[14] Wang, M. D., Schnitzer, M. J., Yin, H., Landick, R., Gelles, J., and Block, S. M., 1998, "Force and Velocity Measured for Single Molecules of RNA Polymerase," Science, **282**, pp. 902–907.
[15] Jean, R. P., Gray, D. S., Spector, A. A., and Chen, C. S., 2004, "Characterization of the Nuclear Deformation Caused by Changes in Endothelial Cell Shape," J. Biomech. Eng., **126**, pp. 552–558.
[16] Caille, N., Thoumine, O., Tardy, Y., and Meister, J. J., 2002, "Contribution of the Nucleus to the Mechanical Properties of Endothelial Cells," J. Biomech., **35**, pp. 177–187.
[17] Theret, D. P., Levesque, M. J., Sato, M., Nerem, R. M., and Wheeler, L. T., 1988, "The Application of a Homogenous Half-Space Model in the Analysis of Endothelial Cell Micropipette Measurements," J. Biomech. Eng., **110**, pp. 190–199.
[18] Tan, J. L., Tien, J., Pirone, D. M., Gray, D. S., Bhadriraju, K., and Chen, C. S., 2003, "Cells Ling on a Bed of Microneedles: An Approach to Isolate Mechanical Force," Proc. Natl. Acad. Sci. U.S.A., **100**, pp. 1484–1489.
[19] Lee, J., Leonard, M., Oliver, T., Ishihara, A., and Jacobson, K., 1994, "Traction Forces Generated by Locomoting Keratocytes," J. Cell Biol., **127**, pp. 1957–1964.
[20] Oliver, T., Dembo, M., and Jacobson, K., 1995, "Traction Forces in Locomoting cells," Cell Motil. Cytoskeleton, **31**, pp. 225–240.
[21] Pienta, K. J., and Coffey, D. S., 1992, "Nuclear-Cytoskeletal Interactions: Evidence for Physical Connections Between the Nucleus and Cell Periphery and Their Alteration by Transformation," J. Cell. Biochem., **49**, pp. 357–365.
[22] Guilak, F., Tedrow, J. R., and Burgkart, R., 2000, "Viscoelastic Properties of the Cell Nucleus," Biochem. Biophys. Res. Commun., **269**, pp. 781–786.
[23] Mogilner, A., and Oster, G., 2003, "Polymer Motors: Pushing Out the Front and Pulling Up the Back," Curr. Biol., **13**, pp. R721–R733.
[24] Dembo, M., and Harlow, F., 1983, "Cell Motility, Contractile Networks, and the Physics of Interpenetrating Reactive Flow," Biophys. J., **50**, pp. 109–121.
[25] Dahl, K. N., and Discher, D. E., 2002, "Micromechanical properties of isolated nuclei and nuclear components," *Annual Fall Meeting of the Biomedical Engineering Society*, p. 144.
[26] Polack, K. J., and Widom, J., 1995, "Mechanism of Protein Access to Specific DNA Sequences in Chromatin: A Dynamic Equilibrium Model for Gene Regulation," J. Mol. Biol., **254**, pp. 130–149.